Instra-Seasonal Oscillation Eastward & Northward propagation

Young-Min Yang, Bin Wang and June-Yi Lee

IPRC, University of Hawaii/Pusan University

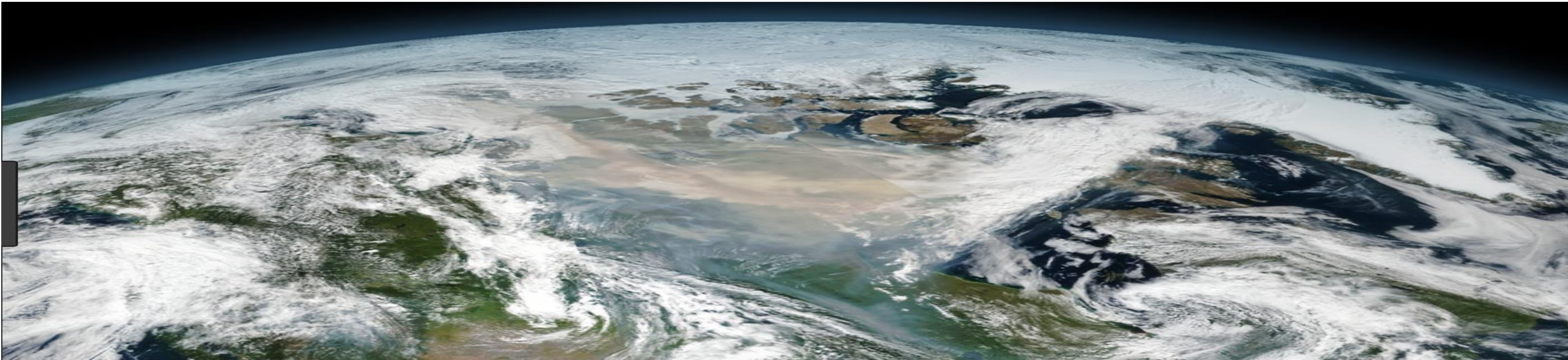

MJO (boreal winter)

- Eastward propagation precipitation with 20-70 days over tropics
- Cyclones, extreme weather event, monsoon and ENSO

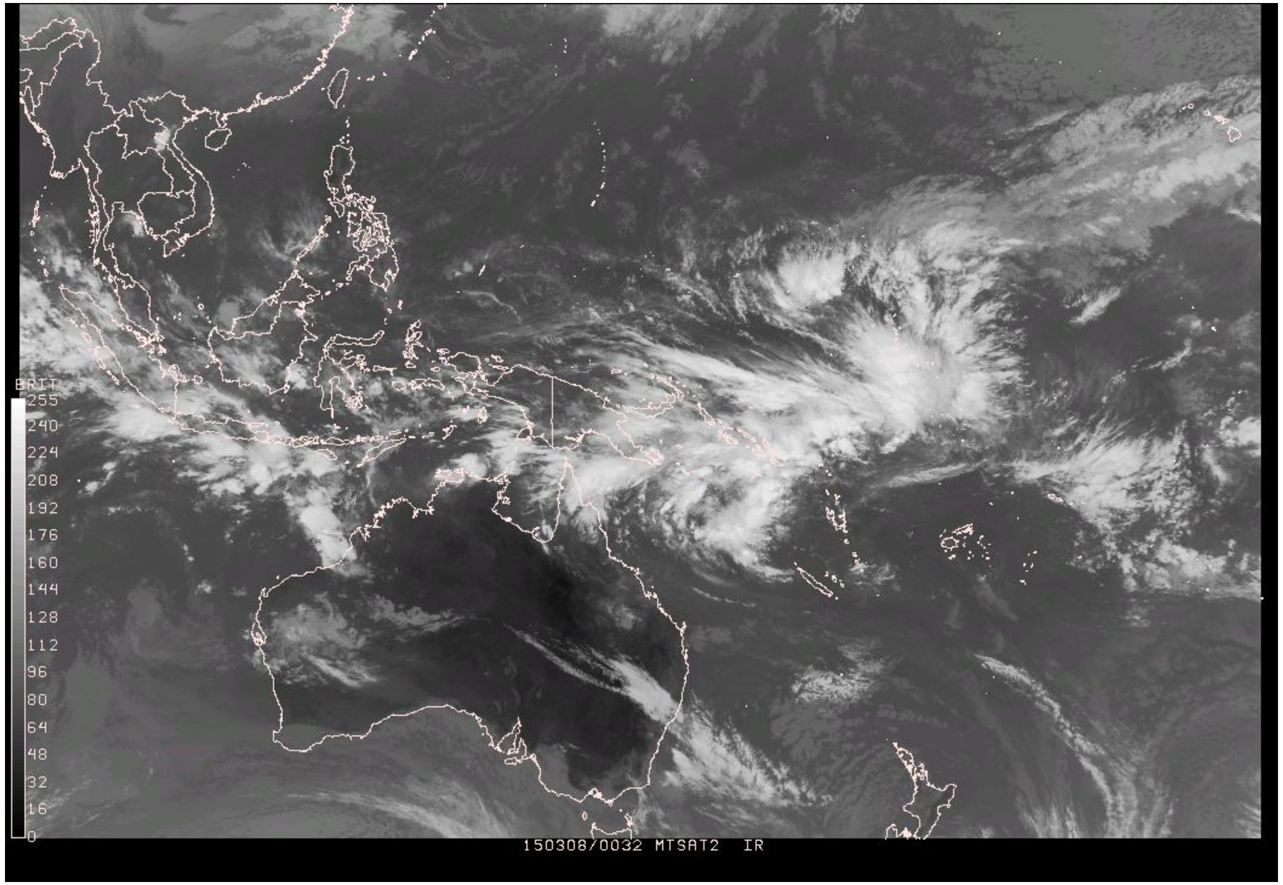

MTSAT-2

MJO tro-interaction theory (Wang et al. 2017)

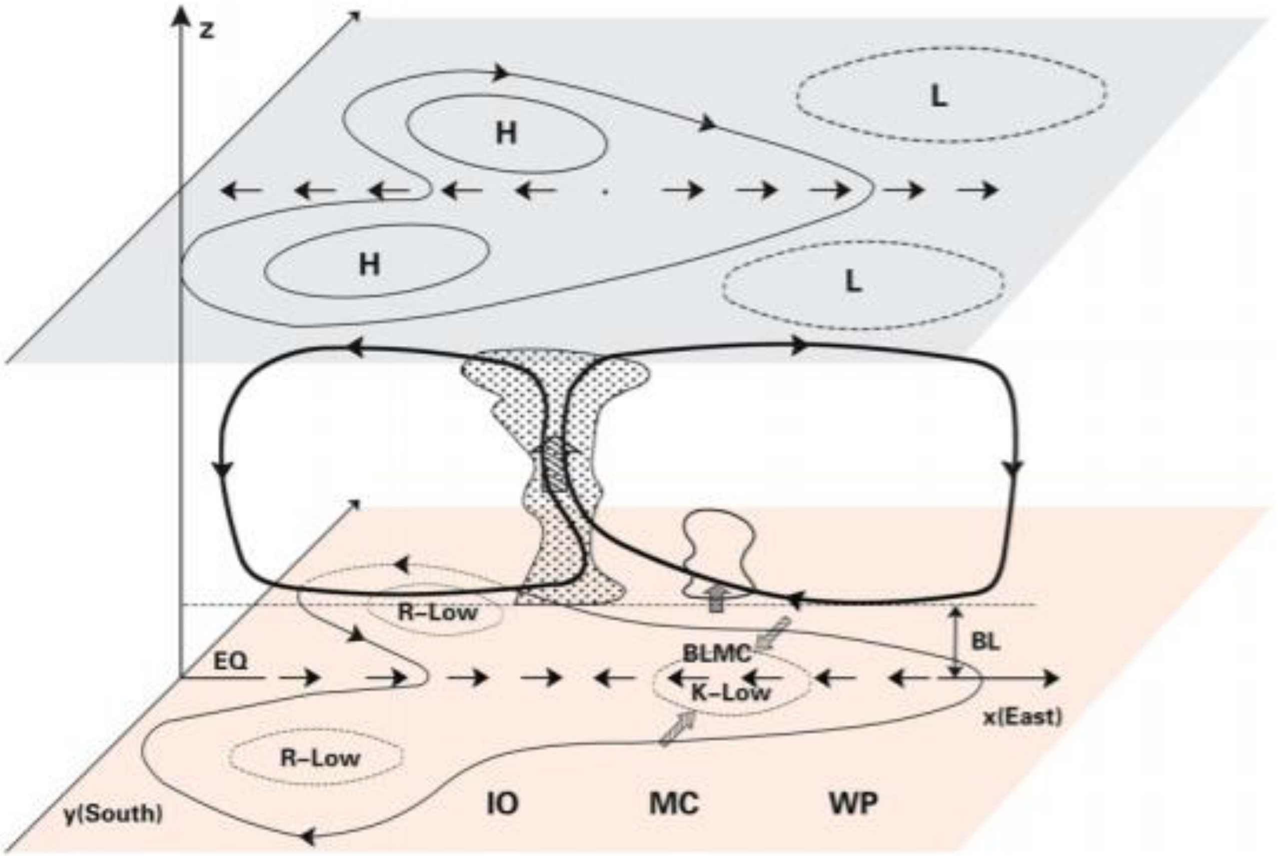

Fig. 1 Schematic diagram illustrating three-dimensional structure of the MJO mode. BLMC represents boundary layer moisture convergence

I. Mean westerly wind

II. K-low at east of MJO convection

III. BL-lower tropospheric interaction

Idealized MJO model – role of boundary layer dynamics (Yang and Wang(2019); Wang et al. (2017)

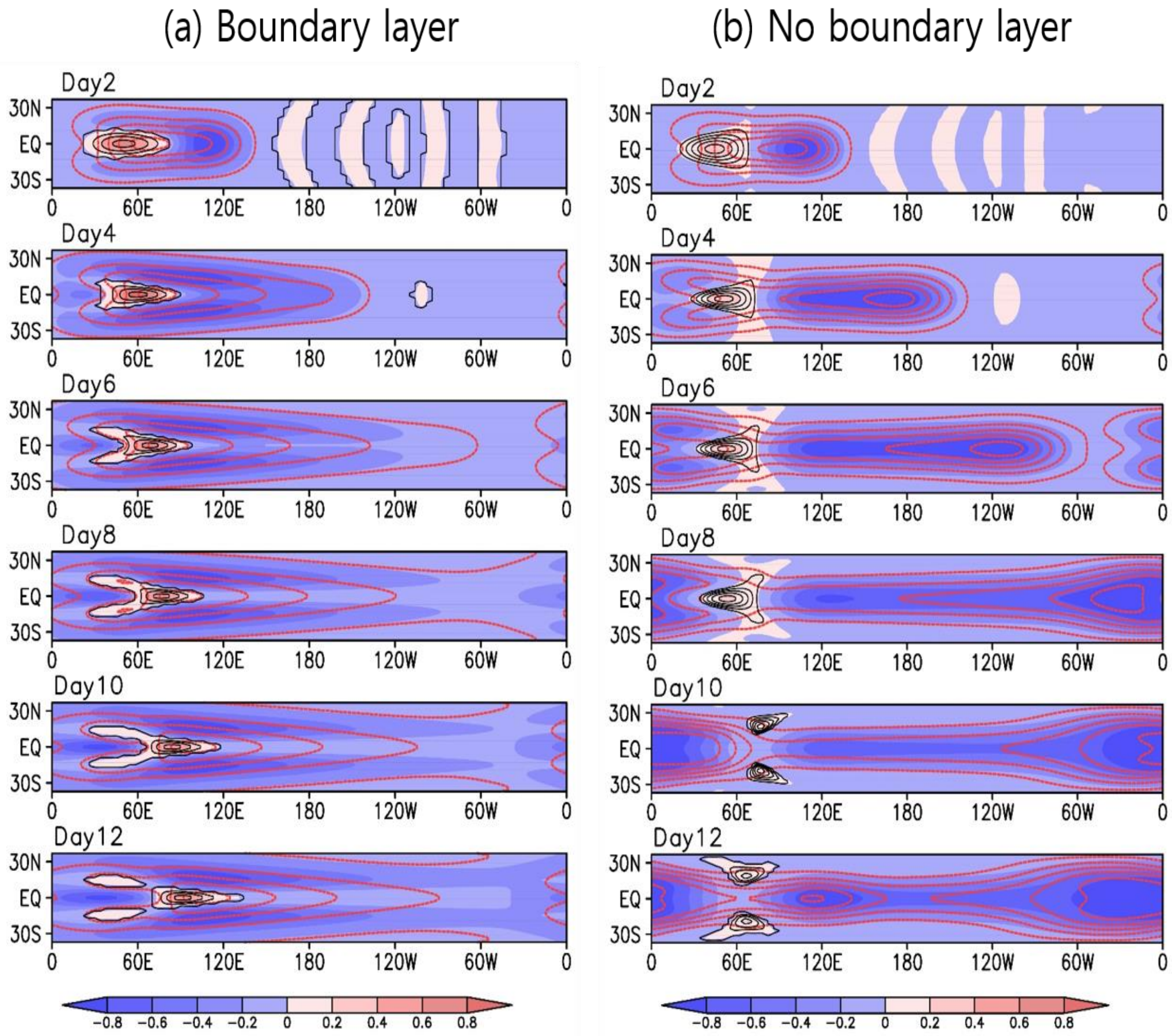

Figure 4 Evolution and horizontal structure of precipitation rate (black line), the lower troposphere geopotential height (red line) and column integrated moisture anomaly (shading) from with the simplified MFC (a) without and (b) with boundary layer dynamics. All fields are normalized by their respective maximum (absolute value) at each panel. The contour interval is 0.1. The geopotential height contours start from - 0.9, and the precipitation contours starts from 0.

Vertical Structure and Diabatic Processes of the MJO: *Global Model Evaluation Project*

MJO Task Force/YOTC and GASS 2012

Lag-regression of rainfall with Indian Ocean base point (70-90E; 5S-5N)

20-100day filtered
dash line – 5 m/s

Jiang et al. 2015

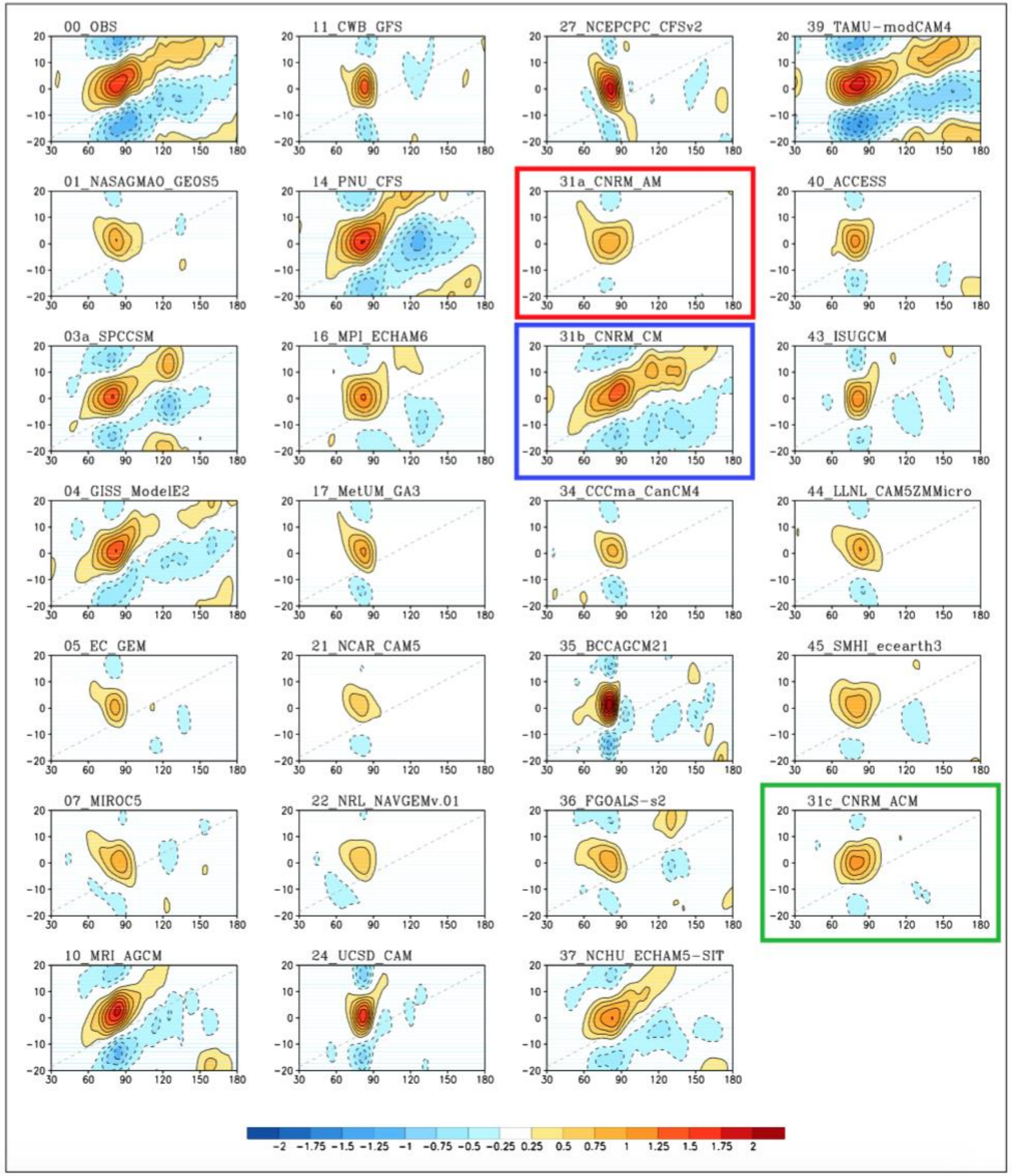

GCM experiments (Yang and Wang. 2018, Clim. Dyn.)

Table.1 Experiments with modified schemes in the NUIST 3.0

Exp.	Convective parameterization	Modified scheme
CTL-TDK	Tiedtke scheme (Tiedtke, 1989)	-
TRG	Tiedtke scheme (Tiedtke, 1989)	BL depth-dependent convective trigger function
SHC	Tiedtke scheme (Tiedtke, 1989)	bottom-heavy diffusivity in the shallow convection scheme
M-TDK	Tiedtke scheme (Tiedtke, 1989)	TRG + SHC
CTL-SAS	Simplified Arakawa-Schubert scheme (Lee et al. 2001)	-
M-SAS	Simplified Arakawa-Schubert scheme (Lee et al. 2001)	TRG +SHC

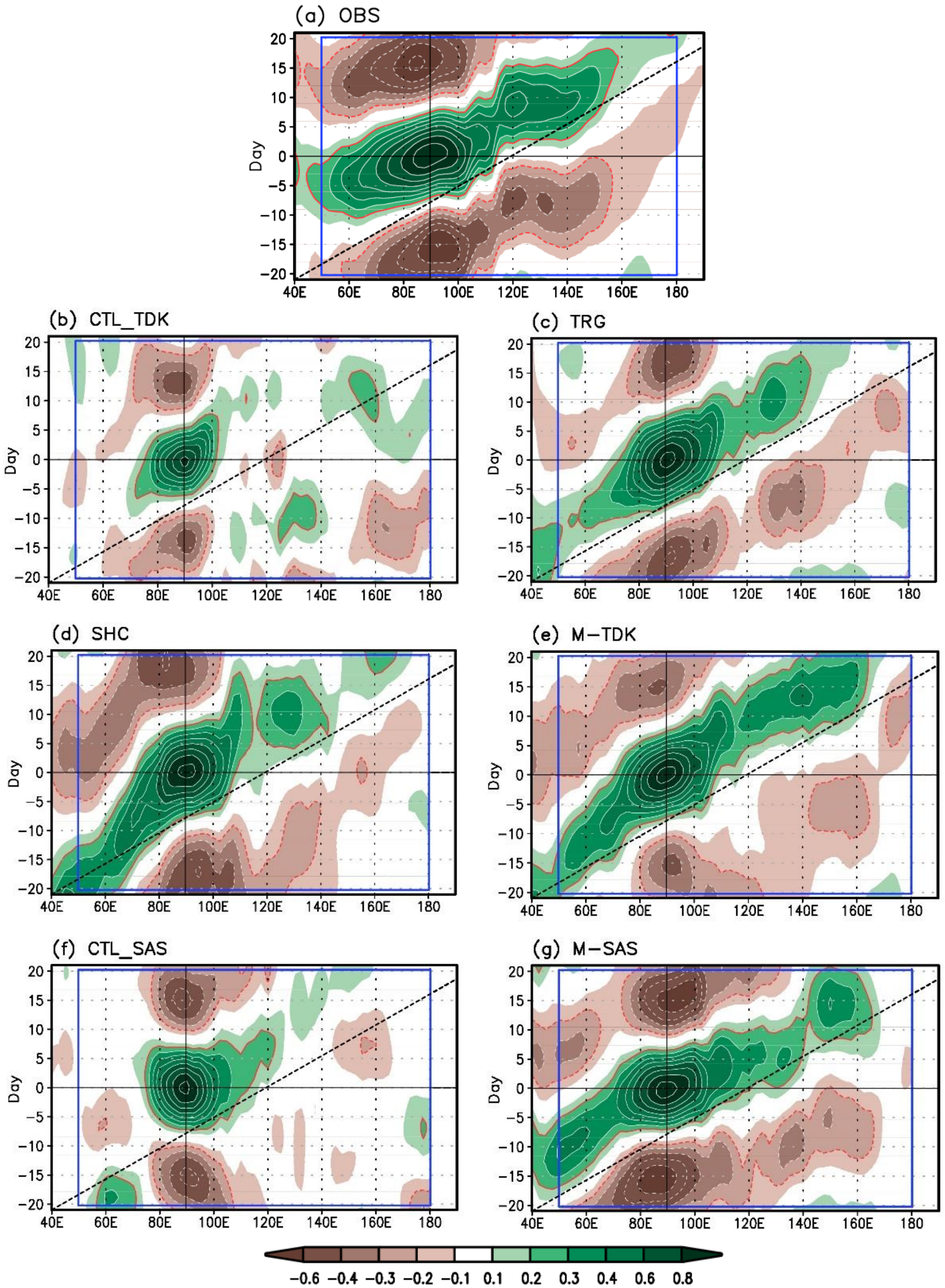

FIG.1 Propagation of MJO precipitation as depicted by the lead-lag correlation of 20-70 day filtered precipitation averaged over 10°S-10°N with reference to the precipitation at the MJO convective center over the equatorial Indian Ocean (10°S-10°N, 80°-100°E) during boreal winter (NDJFMA) derived from (a) observation and model simulations in the experiments of (b) CTL-TDK, (c) TRG, (d) SHC, (e) M-TDK, (f) CTL-SAS and (g) M-SAS. The red contour represents the correlation coefficient of ±0.2. Black dotted lines indicate eastward propagation speed of 5 m s^{-1}. The black rectangular line represent the area used for PCC. Horizontal black line is lag of 0 and vertical black line is longitude of 90°E.

Wavenumber-frequency spectra

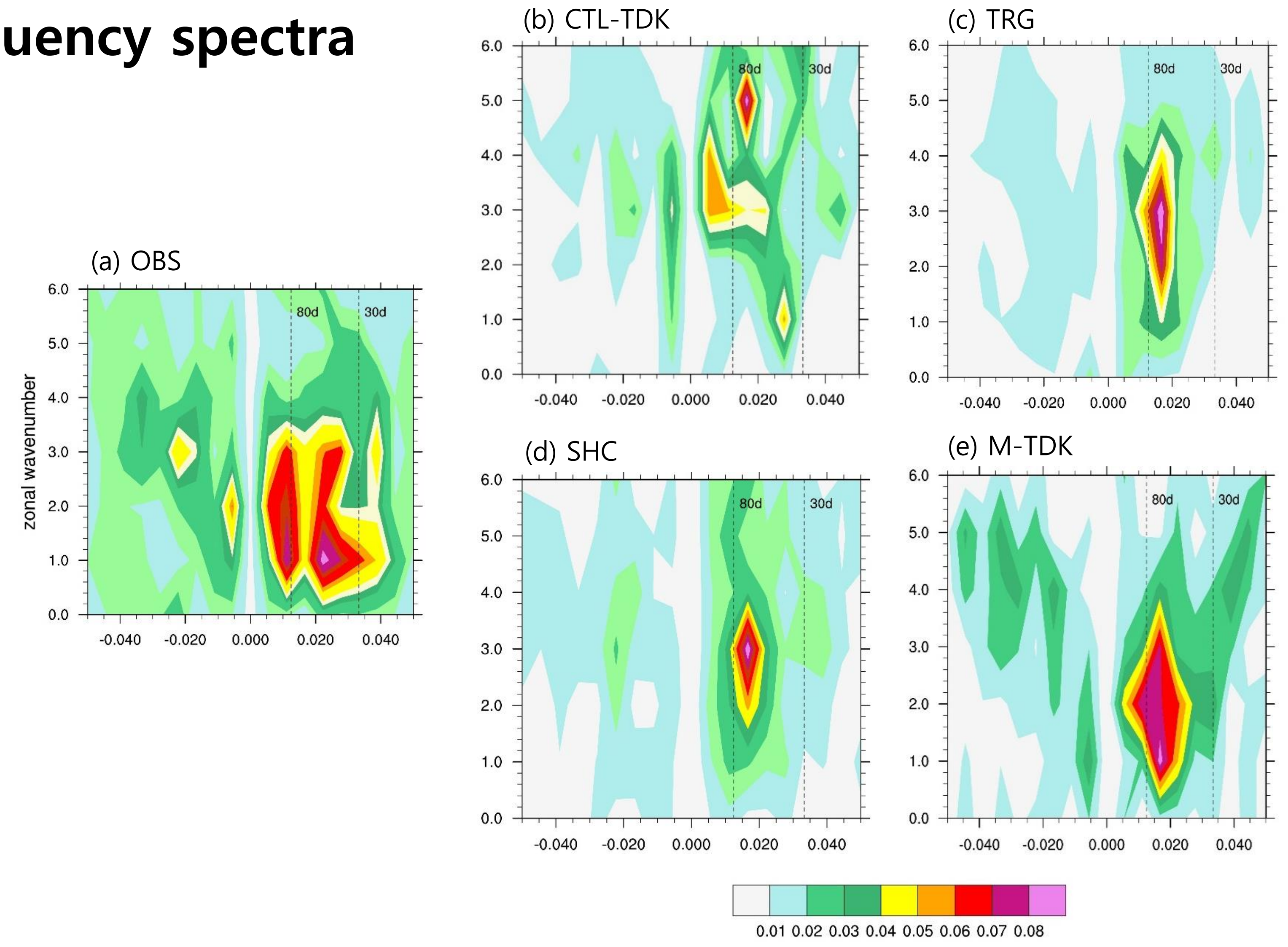

FIG 5. November–April wavenumber-frequency spectra of 10°N–10°S-averaged (a) GPCP precipitation and (b)-(e) models. Only the climatological seasonal cycle and time mean for each November-April segment were removed before calculation of the spectra. Units for the spectrum are mm^{-2} day^{-2}

Change of Mean state

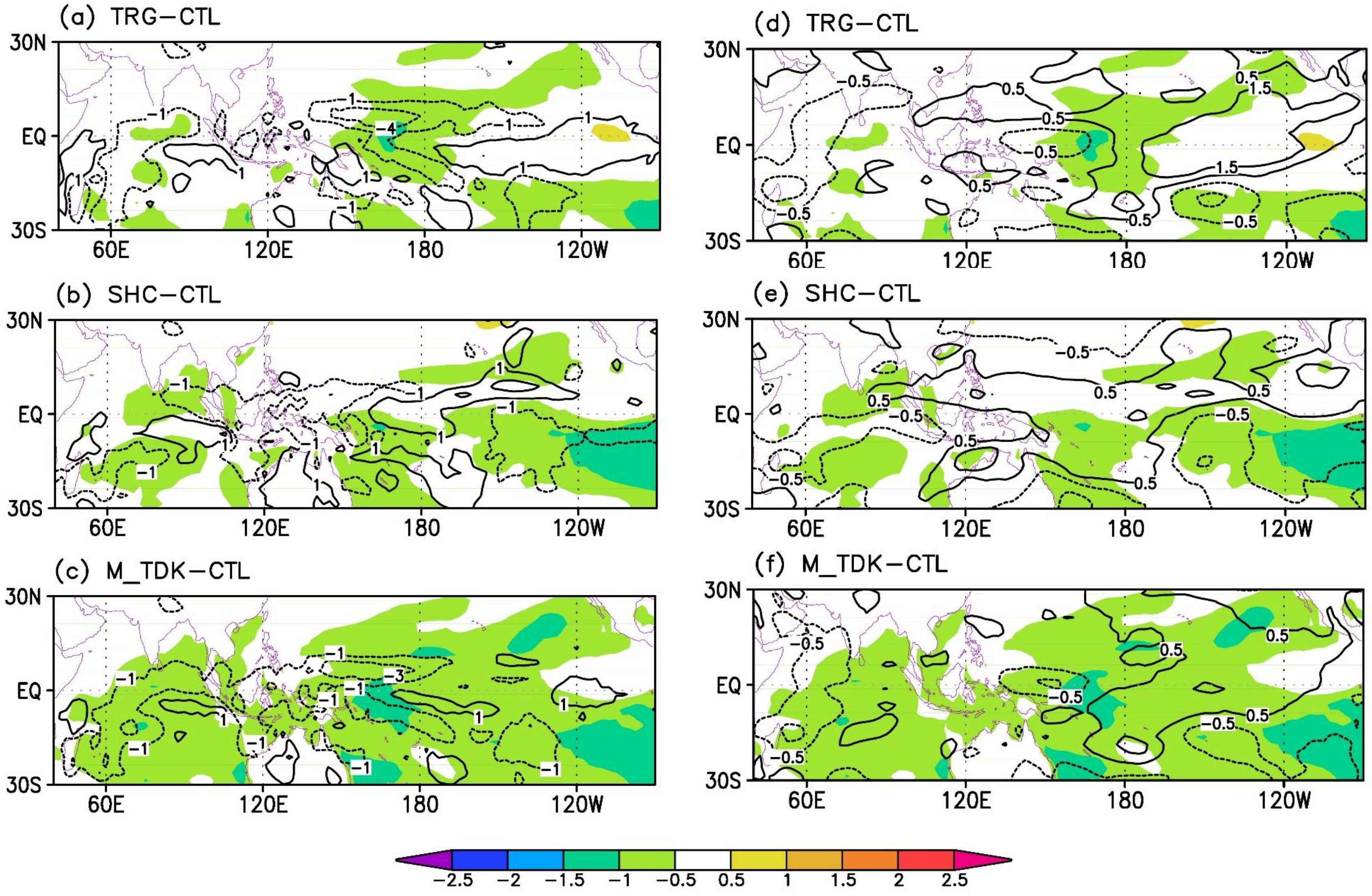

FIG. 2 difference of November-April mean temperature (shading), precipitation (contour, a-c) and surface zonal wind (contour, d-f) between CTL and TRG, SHC and M-TDK

Regressed diabatic heating at 850hPa

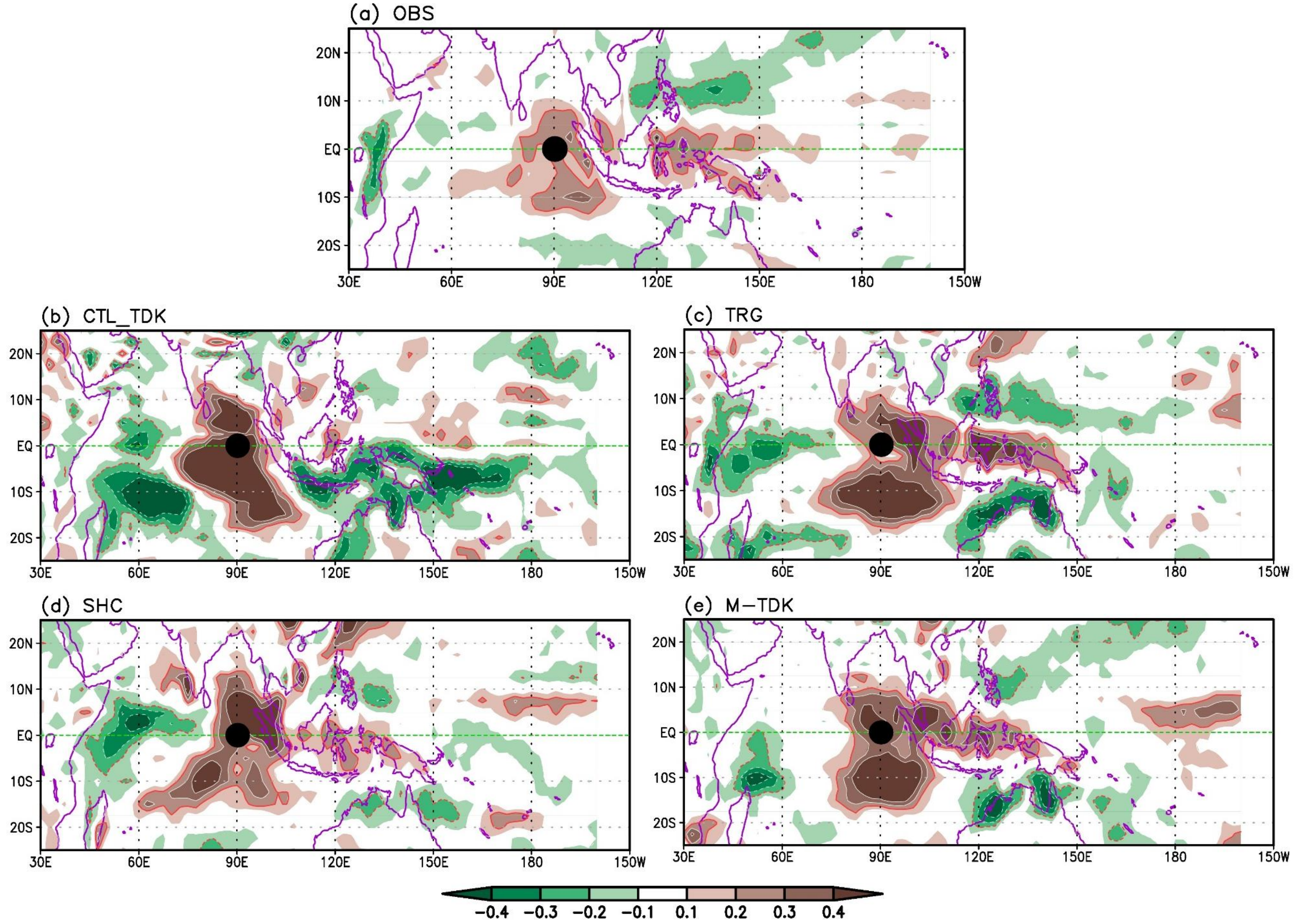

FIG.6 Horizontal structure of diabatic heating at 700hPa in observation (a) and model simulations (b)-(e) depicted by the regressed 20-70 day filtered diabatic heating (K day^{-1}) onto the 20-70 day filtered precipitation averaged over the MJO precipitation center (10°S-10°N, 80°-100°E), which is symbolized by the black filled circle. The regression strengths are scaled to a fixed 3mm day^{-1} precipitation rate. The red contour represents the regression coefficient of ±0.2. Green horizontal line is equator.

Horizontal structure of circulation

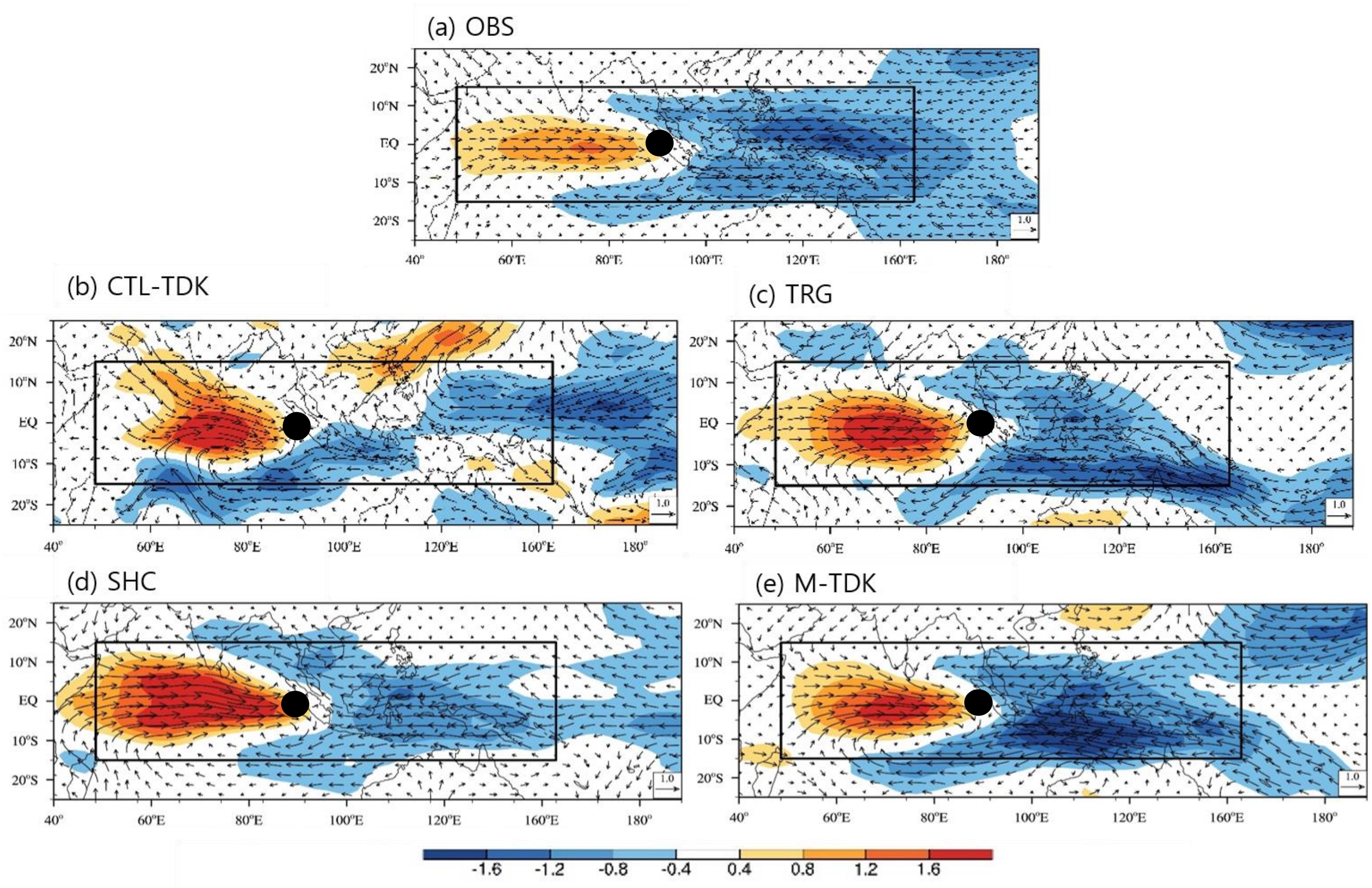

FIG. 8 The same as in Fig. 3 except for the 850hPa winds (m s^{-1}, vector) and 850 hPa zonal wind speed (U850) (m s^{-1}, shading). The rectangular line represents the area used for PCC

Regressed BLMC at 925hPa

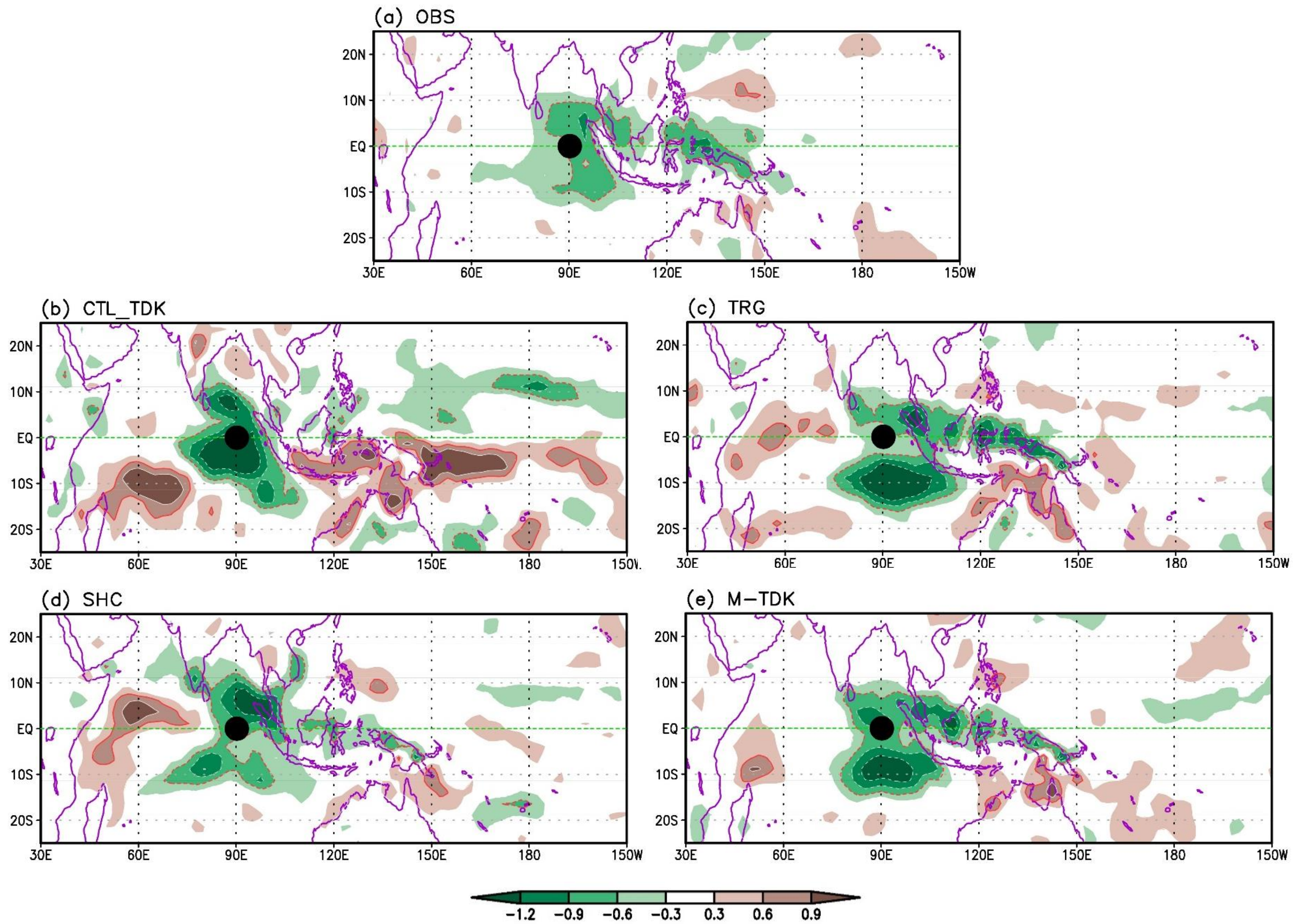

FIG.9 The same as in Fig. 3 except for the moisture convergence at the 925hPa (day^{-1}). The red contour represents the regression coefficient of ±0.6.

Vertical profile of EPT (shading) & moisture (contour)

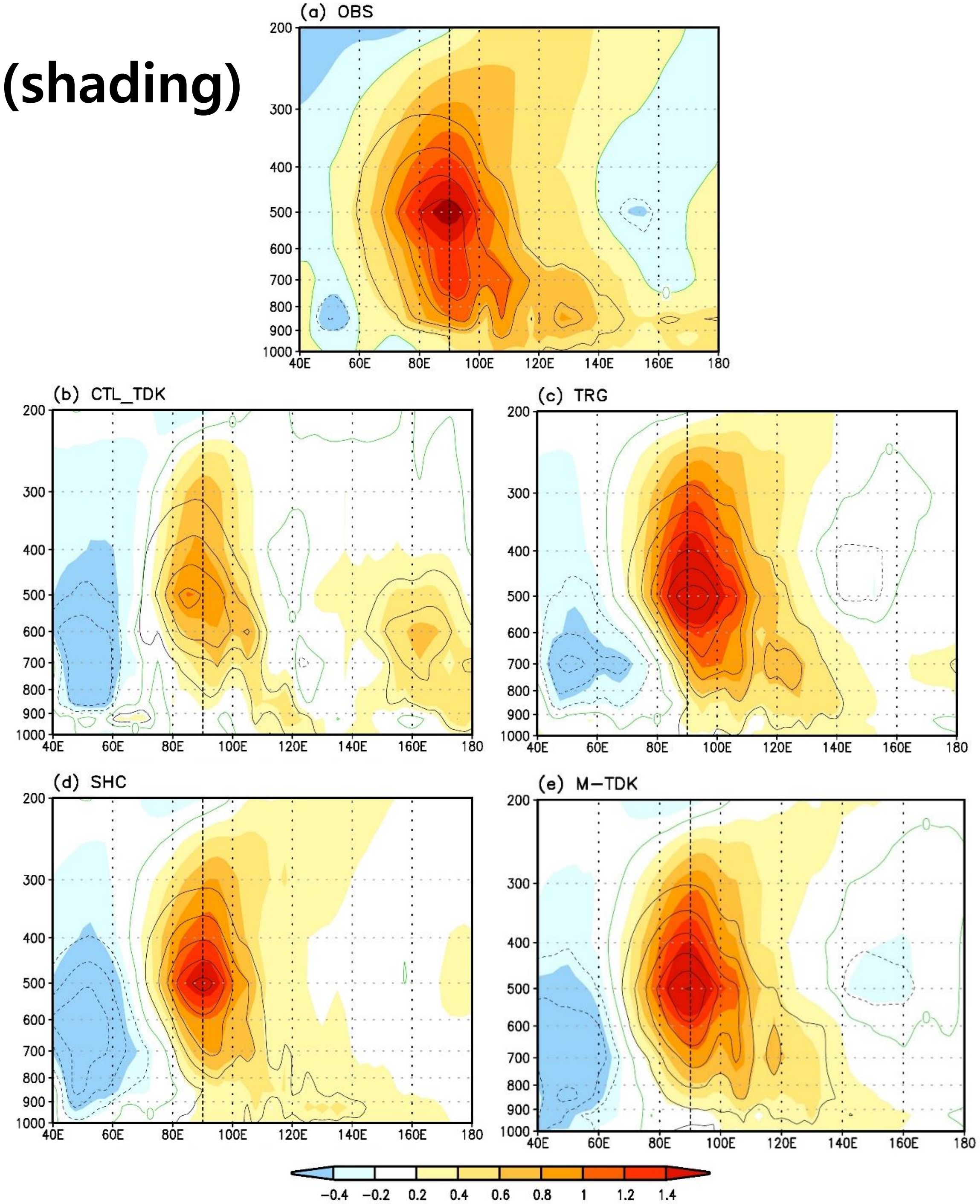

FIG.10 The same as in Fig. 4 except for equivalent potential temperature (EPT) (K, shading) and specific humidity (g kg^{-1} , black contour, CI=0.1) averaged between 5°S and 5°N. Green contour represents the regression coefficient of 0.

Vertical profile of eddy APE (contour) & temperature (shading)

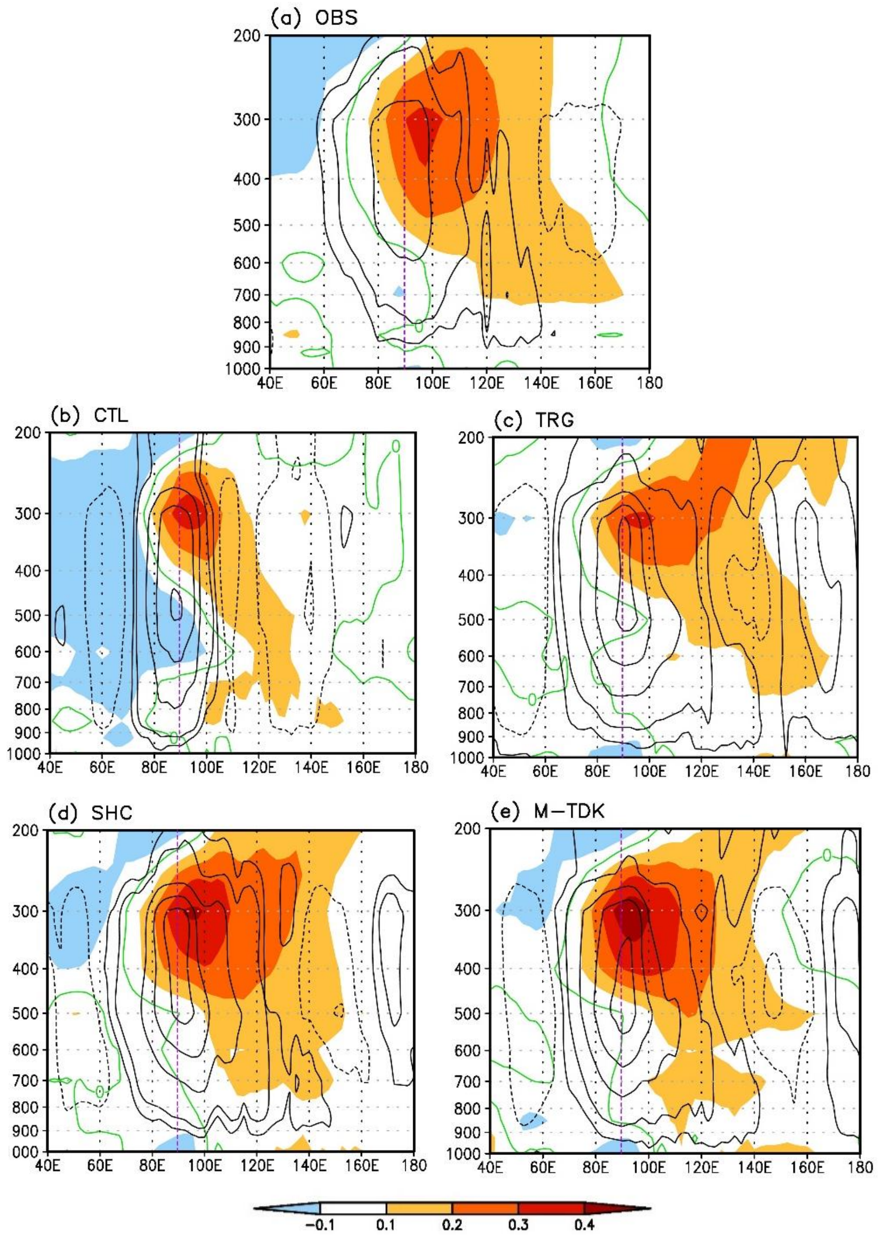

FIG.12 The same as in Fig. 4 except for the MJO available potential energy (APE) generation rate (K^2 day^{-1}, contour) and temperature anomalies (K, shading) averaged between 5°S and 5°N. Green contour represents the regression coefficient of 0. Contour starts from -100 with 200 interval.

SAS scheme : Diabatic heating, Circulation and BLMC

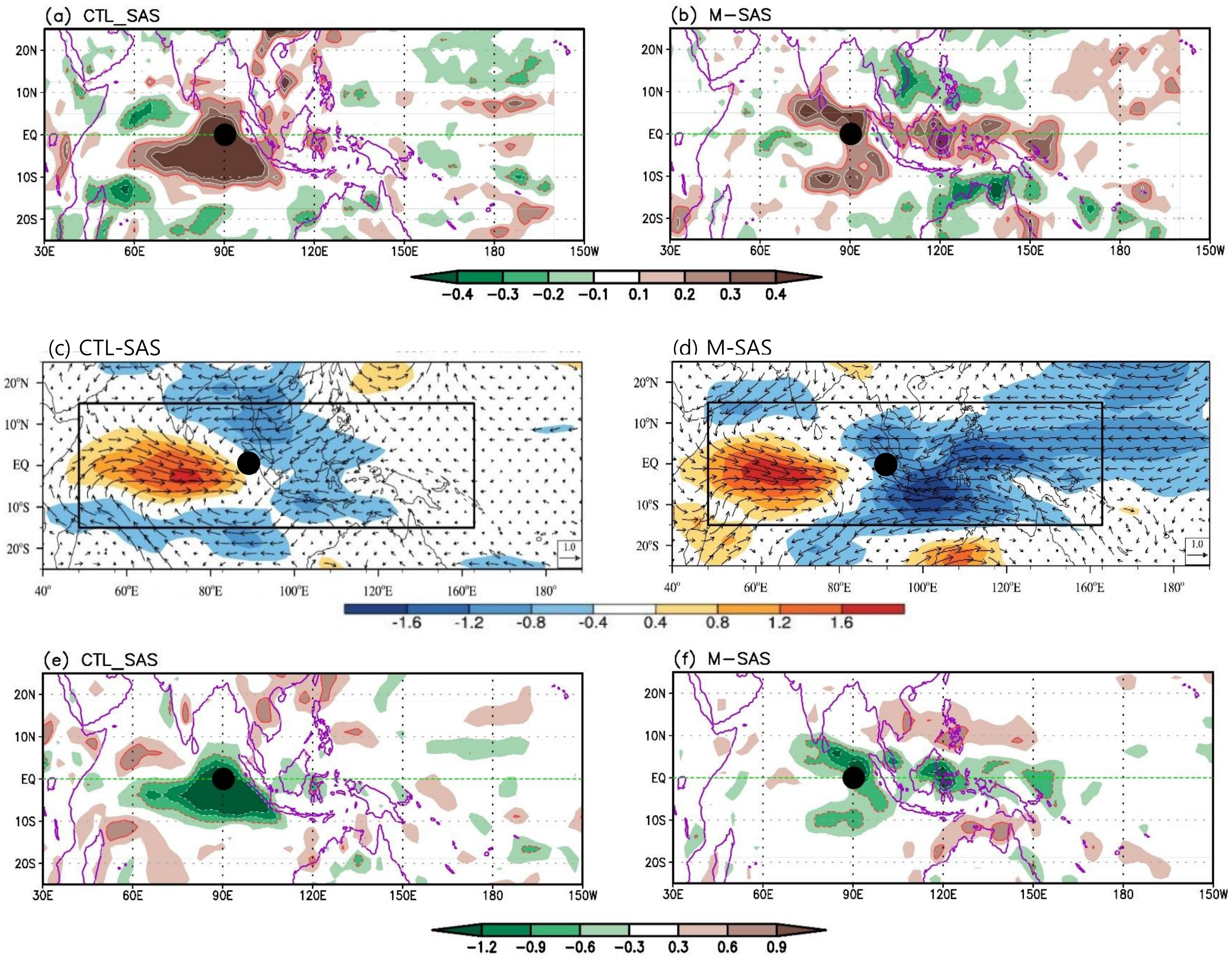

Fig. 14 Comparison of the dynamic structures simulated in CTL-SAS and M-SAS. (a) and (b) Horizontal structure of diabatic heating (K day^{-1}) at 700 hPa in C-SAS and M-SAS. (c) and (d) Horizontal structure of 850 hPa wind (m s^{-1}, vector) and 850 hPa zonal wind speed (U850) (m s^{-1}, shading) in C-SAS and M-SAS. (e) and (f) horizontal structure of boundary layer moisture convergence (day^{-1}) at 925 hP in C-SAS and M-SAS. The structures are regressed 20-70 day band pass filtered fields with reference to the MJO precipitation anomaly in the equatorial Indian Ocean (10S-10N, 80-100E), which is symbolized by the black filled circle. . The regression strengths are scaled to a fixed 3mm day^{-1} precipitation rate. The rectangular line represents the area used for PCC

Diabatic heating & eddy APE

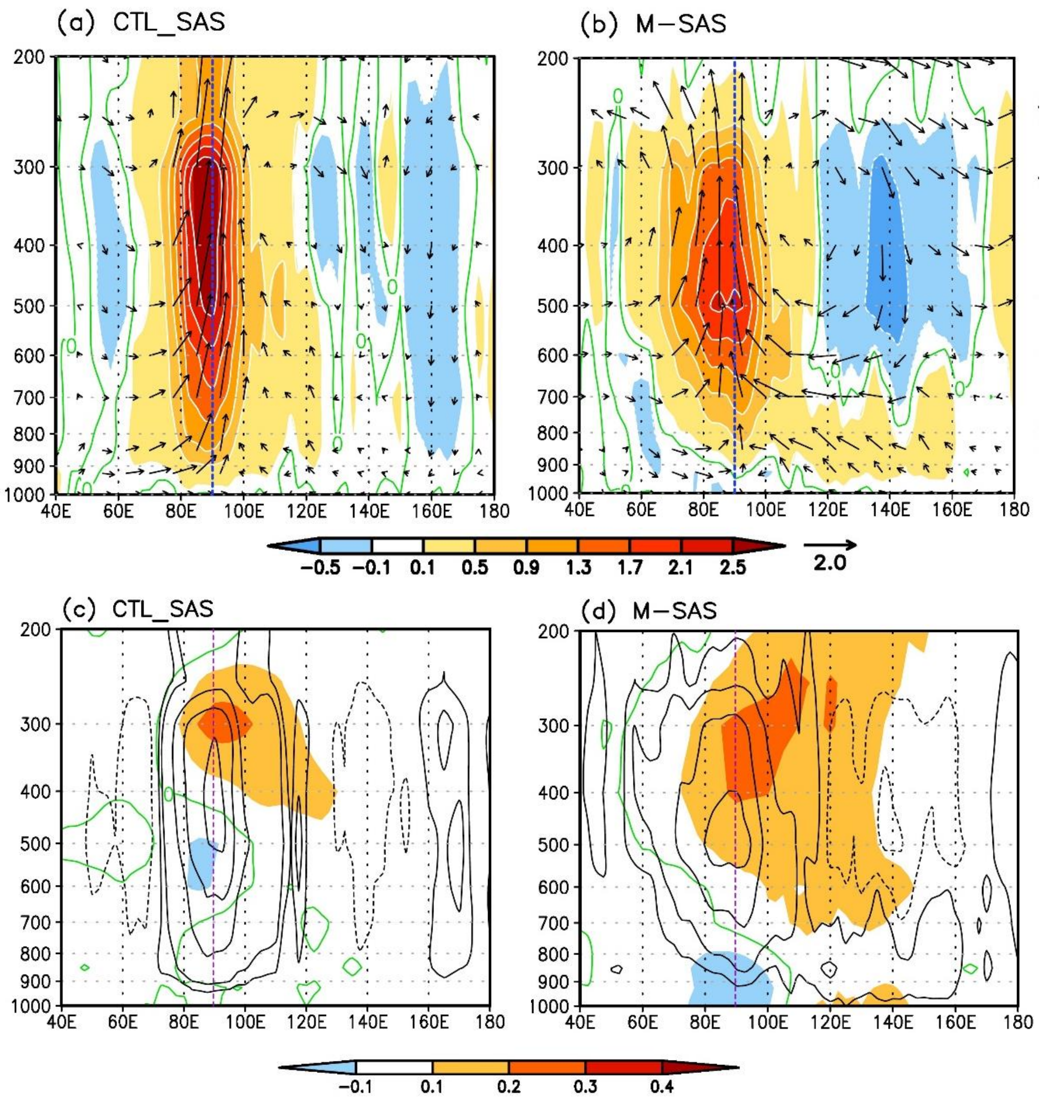

FIG.15 Comparison of the vertical structures simulated in CTL-SAS and M-SAS. (a) and (b) diabatic heating (K day^{-1}, shading) and anomalous Walker cell (m s^{-1} for zonal wind and 0.01 Pa s^{-1} for vertical velocity, vector) averaged between 5°S-5°N. (c) and (d) Eddy available potential energy (APE) generation rate (K^{2} day^{-1}, contour) and temperature anomalies (K, shading) averaged between 5°S-5°N. The structures are regressed 20-70 day band pass filtered fields with reference to the precipitation anomaly in the equatorial Indian Ocean (10S-10N, 80-100E). The regression strengths are scaled to a fixed 3mm day^{-1} precipitation rate and averaged over 5S-5N. The intervals of contour in (c) and (d) are same as that of shading. Green contour represents the regression coefficient of 0. Contour starts from -100 with 200 interval.

Schematics for eastward propagation of MJO

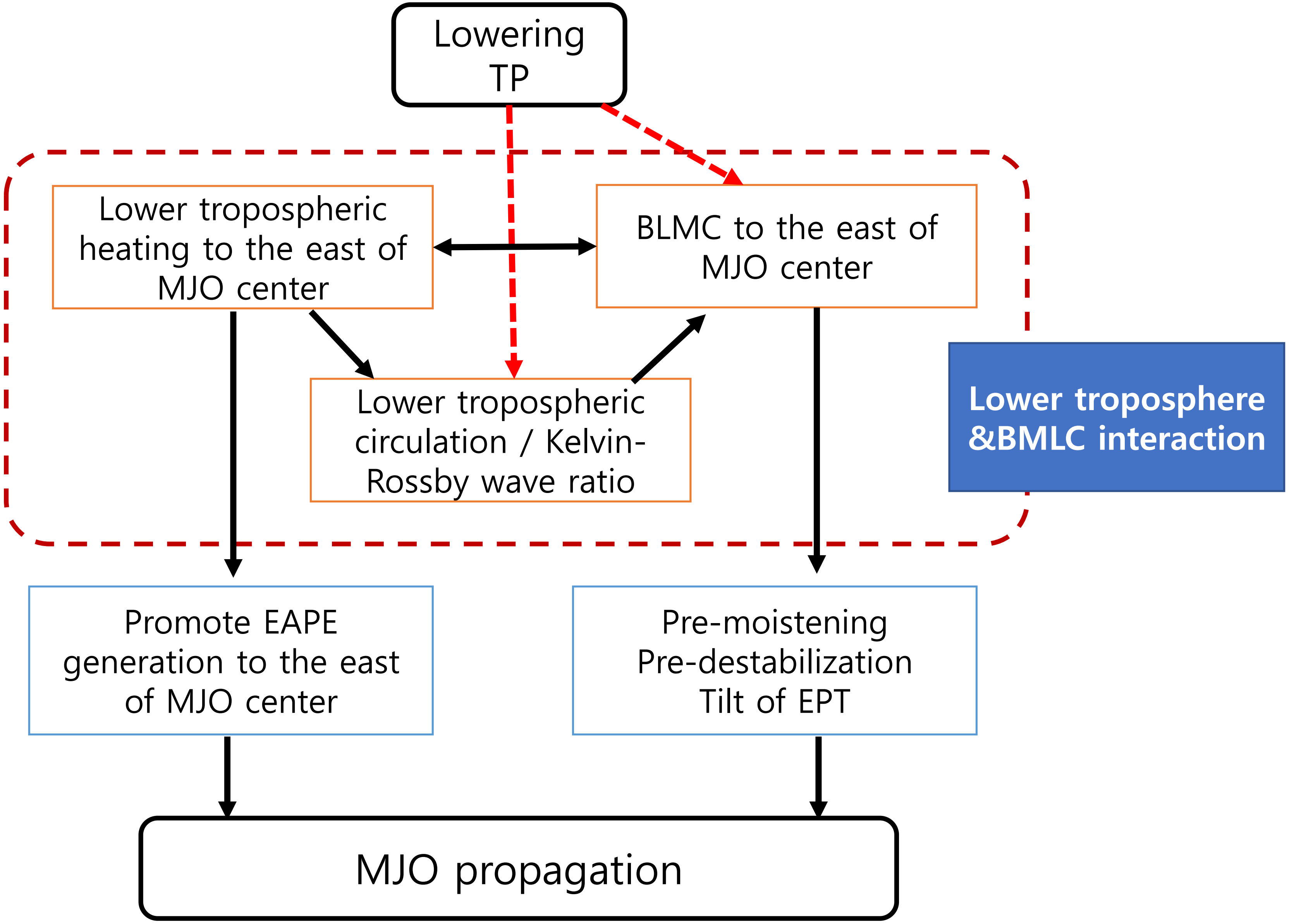

The Tibetan Plateau Uplift is Crucial for Eastw ard Propagation of Madden-Julian Oscillation?

Yang et al. 2019, GRL (Accepted)

Boreal Summer Intra-Seasonal Oscillation (BSISO)

- Northward propagation precipitation with 1.0 m/s over EIO and WP
- Monsoon onset, rain belt, cyclone, extratropical circulation
- Voriticity by vertical shear/ meridional gradient of mean moisture or V-wind/ Air-Sea interaction (meridional gradient of SST)

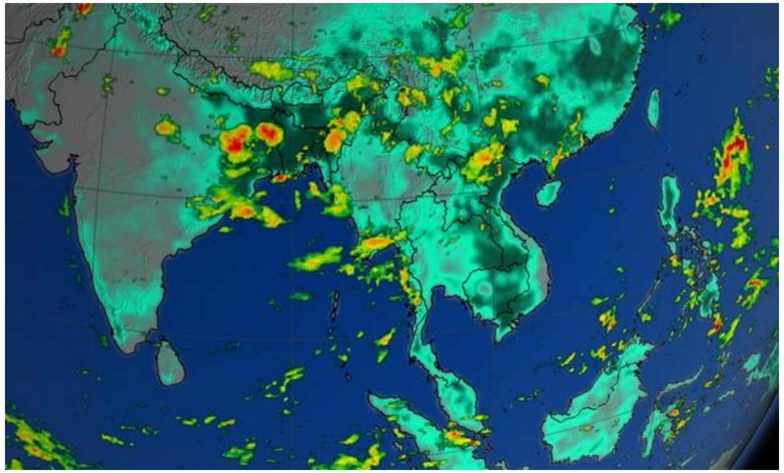

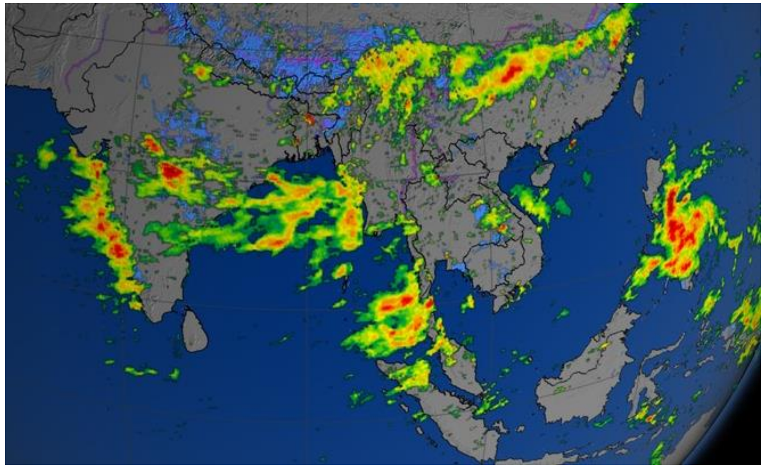

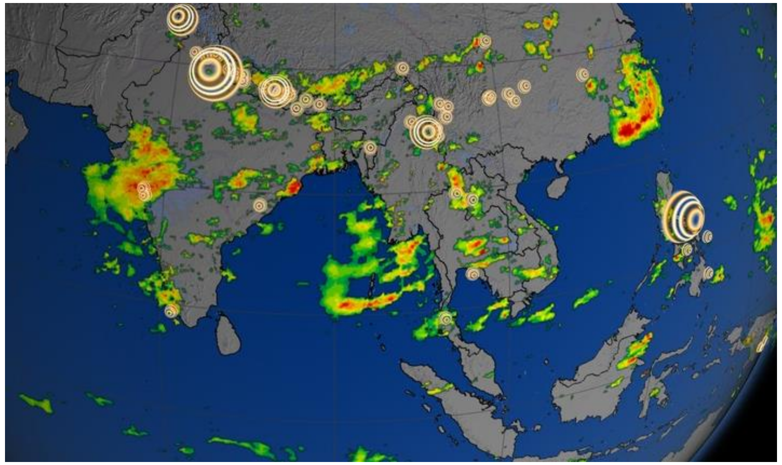

Mechanism for northward propagation

(Vorticity anomalies by zonal vertical shear, Xiang et al. 2004)

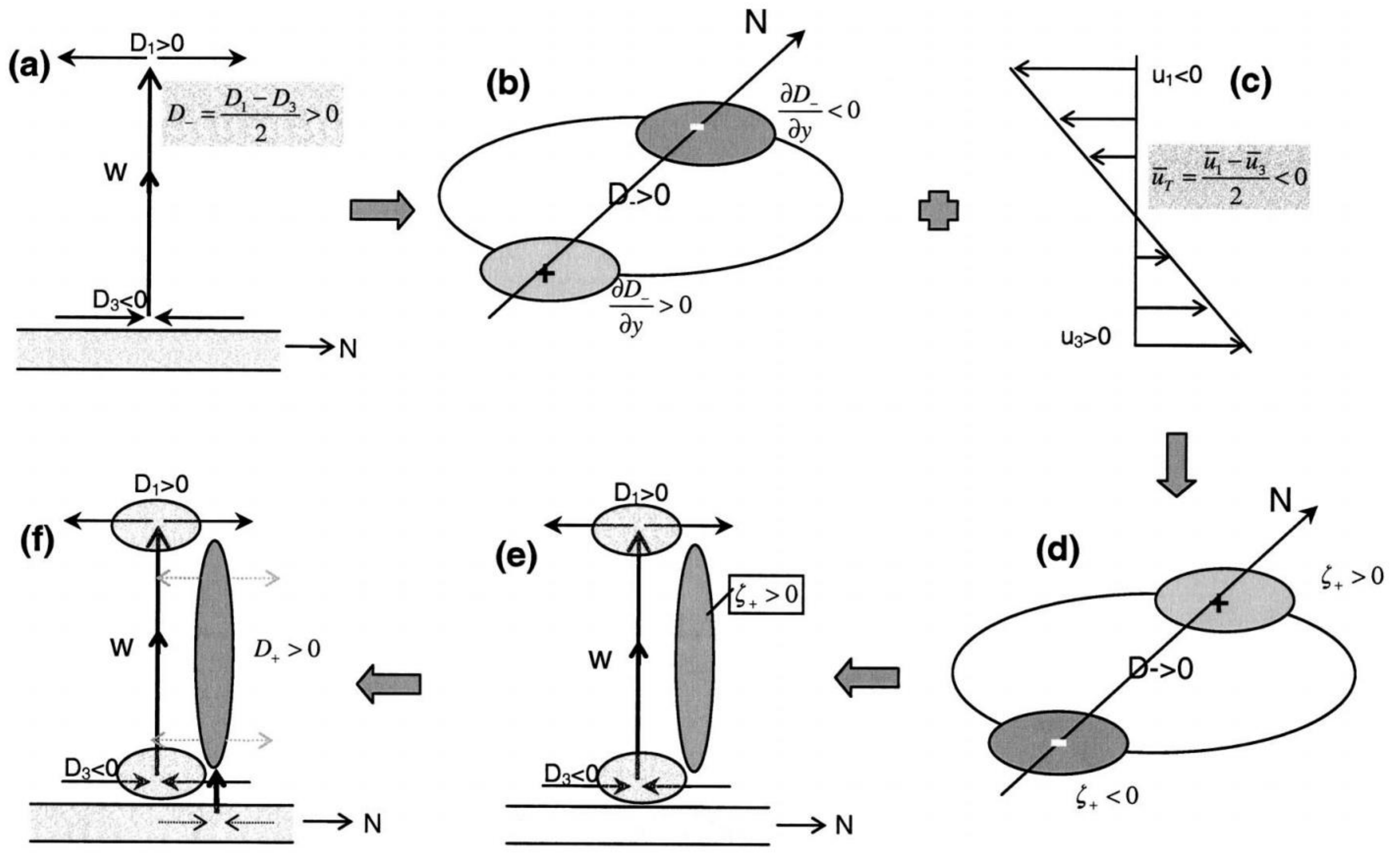

FIG. 10. Schematic diagram for the vertical shear mechanism. (a) Consider initially an ISO convection with a baroclinic structure. (b) This leads $\partial D_-/\partial y < 0$ ($\partial D_-/\partial y > 0$) north (south) of the convection center. (c) In the presence of the easterly shear of the mean flow, (d), (e) a positive barotropic vorticity is induced north of the convection, leading to (f) a barotropic divergence in situ. The latter further leads to a PBL convergence and thus a northward shift of convective heating.

Mountain Lift experiment (Tibetan Plateau, TP)

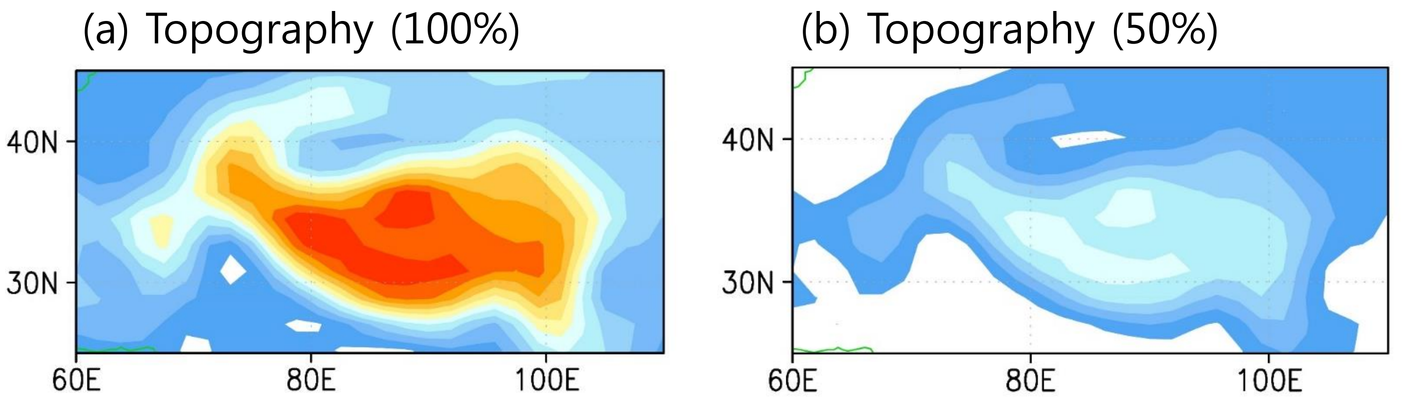

Main questions

1) lowering TP affects MJO or BSISO simulation?

2) How lowering TP change MJO or BSISO?

Model : NESM3.0 (atmosphere (ECHAM6.3)-ocean (NEMO3.0)-Land(JSBACH)-Seaice(CICE4.0)
- 1990's fixed forcing (GHG, aerosol, vocanic, ozone, land use, solar forcing)
- freely coupled, No flux correction
- 20year simulations

Northward propagation of MJO at East Indian Ocean (boreal summer)

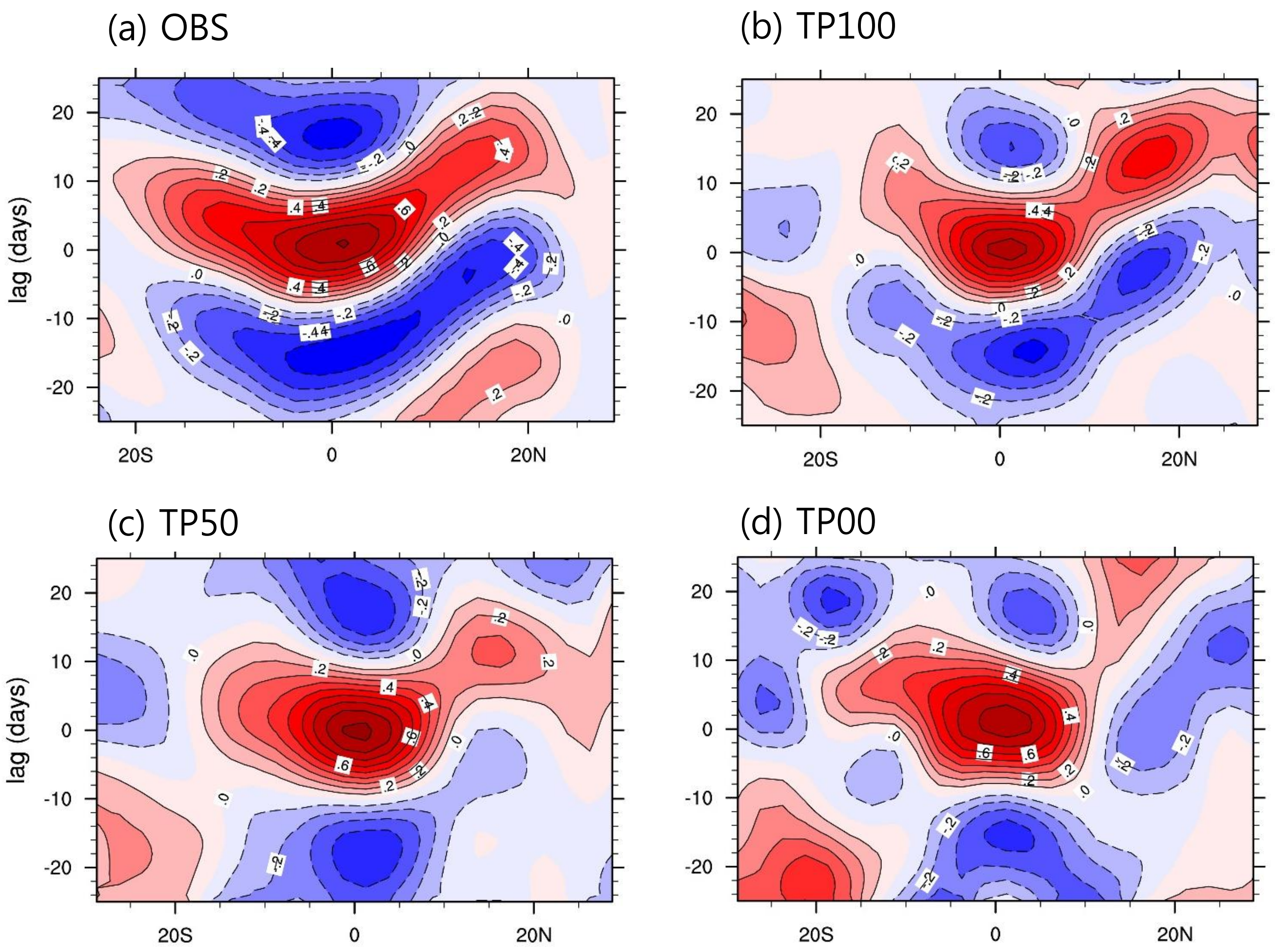

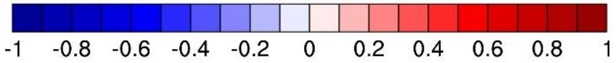

FIG.3 Propagation of ISO precipitation as depicted by the lead-lag precipitation averaged over 80°-100°E with reference to the precipitation at the ISO convective center over the equatorial Indian Ocean (5°S-5°N, 80°-100°E) during boreal summer (MJJASO) derived from (a) observation and model simulations in the experiments with (b) observed topography, (c) 50% of observed topography and (d) no topography over Tibet region.

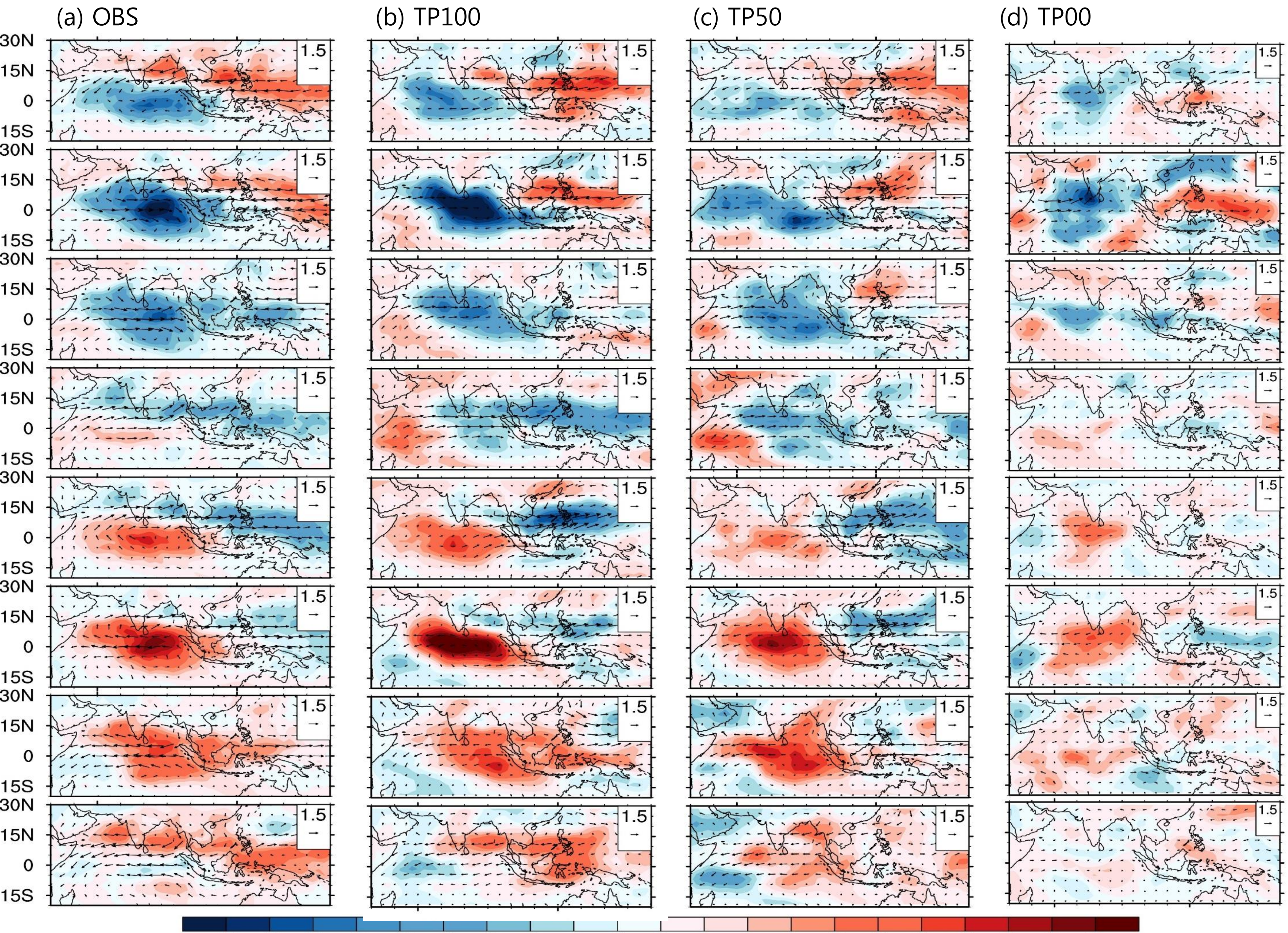

Fig. 2 The life cycle composite of OLR (shading) and 850-hPa wind (vector) anomaly reconstructed based on PC1 and PC2 of BSISO1 in 8 phases. The composite life cycles with moderate amplitude (1.0). We defined 8 phase of ISO based on Lee et al. (2013) that make its related composite fields based on the magnitudes and signs of the PC1 and PC2 of the BSISO OLR and zonal wind at 850hPa. Top (bottom) panel represents phase1 (phase8).

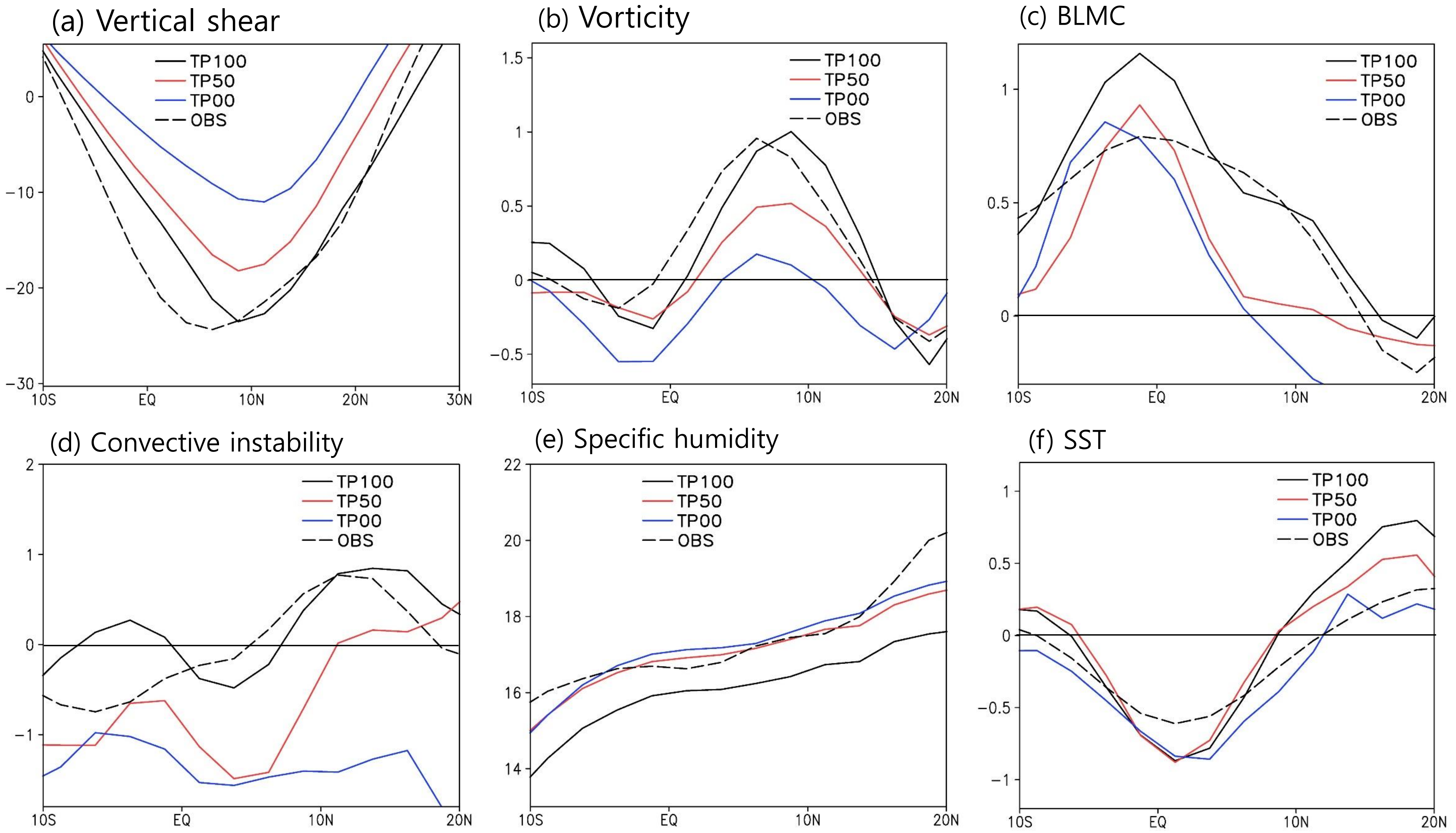

FIG. 4 Meridional structure of May-November (a) mean zonal shear (U_{200} - U_{850}) and (e) mean specific humidity averaged over 80˚-100˚E from observation (dashed black) and models (colored line). Meridional variation of the regressed ISO (b) relative vorticity (s^{-1}) at 850 hPa, (c) BL moisture convergence (day^{-1}) at 925hPa (d) convective instability index and (f) SST averaged 80°-100°E onto the 20-70 day filtered precipitation averaged over the IO center (5°S-5°N, 80°-100°E) from observation (dashed black) and model simulations (colored line). The regression strengths are scaled to a fixed 3mm day-1 precipitation rate.

Thank you!

Difference of mean state in SST, PRCP & Wind

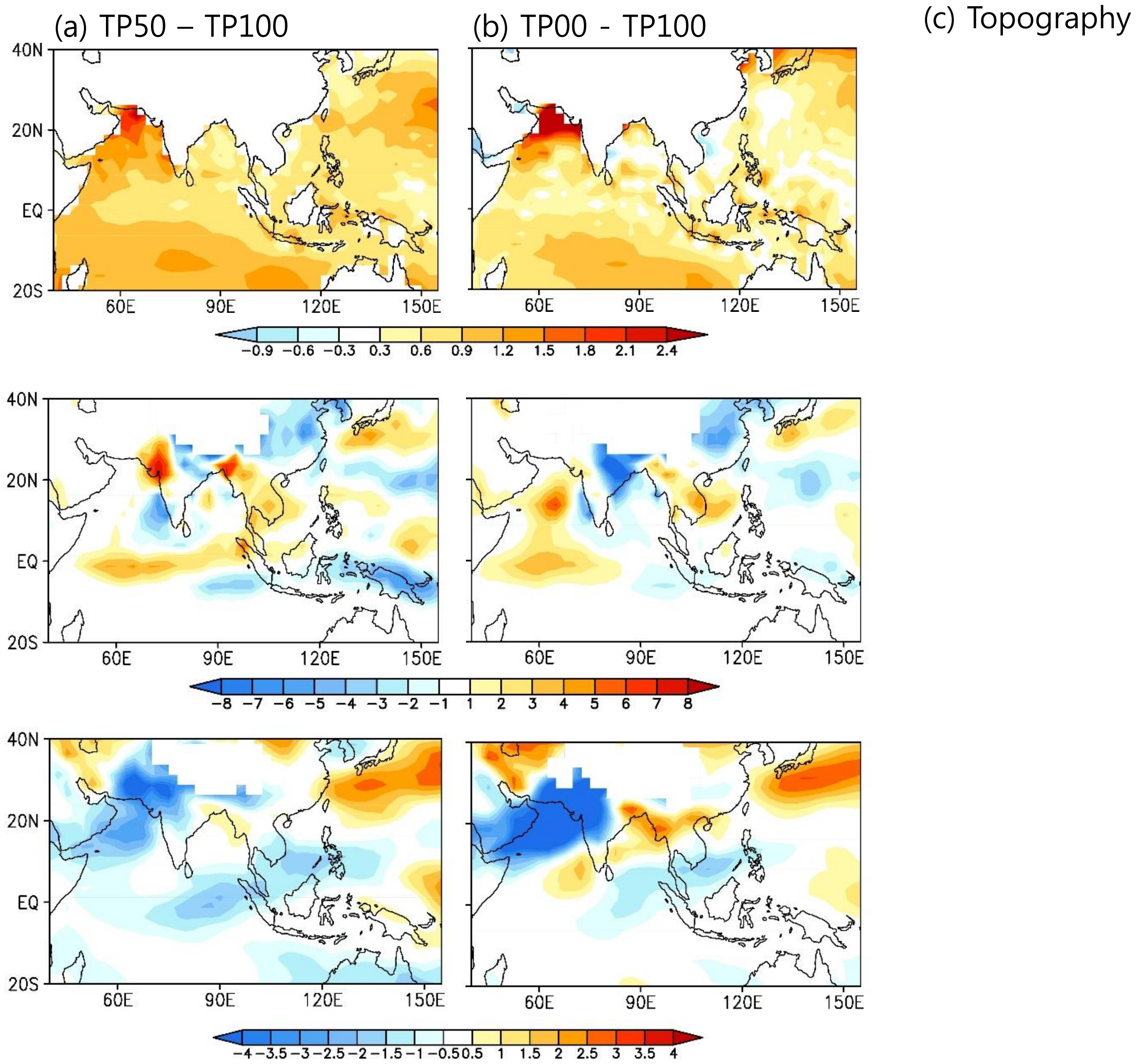

FIG. 1 Difference of July-August mean-state sea surface temperature (K, shading) (upper panel), precipitation (mm day^{-1}, red contour) (middle panel) and zonal wind at 850 hPa (m s^{-1}, blue contour) (lower panel) between (a) TP50 and (b) TP00 and TP100. (c) Horizontal map of orography (m) over Tibet plateau region used in the Original (observed, upper panel) and reduced (50%) value (middle panel).

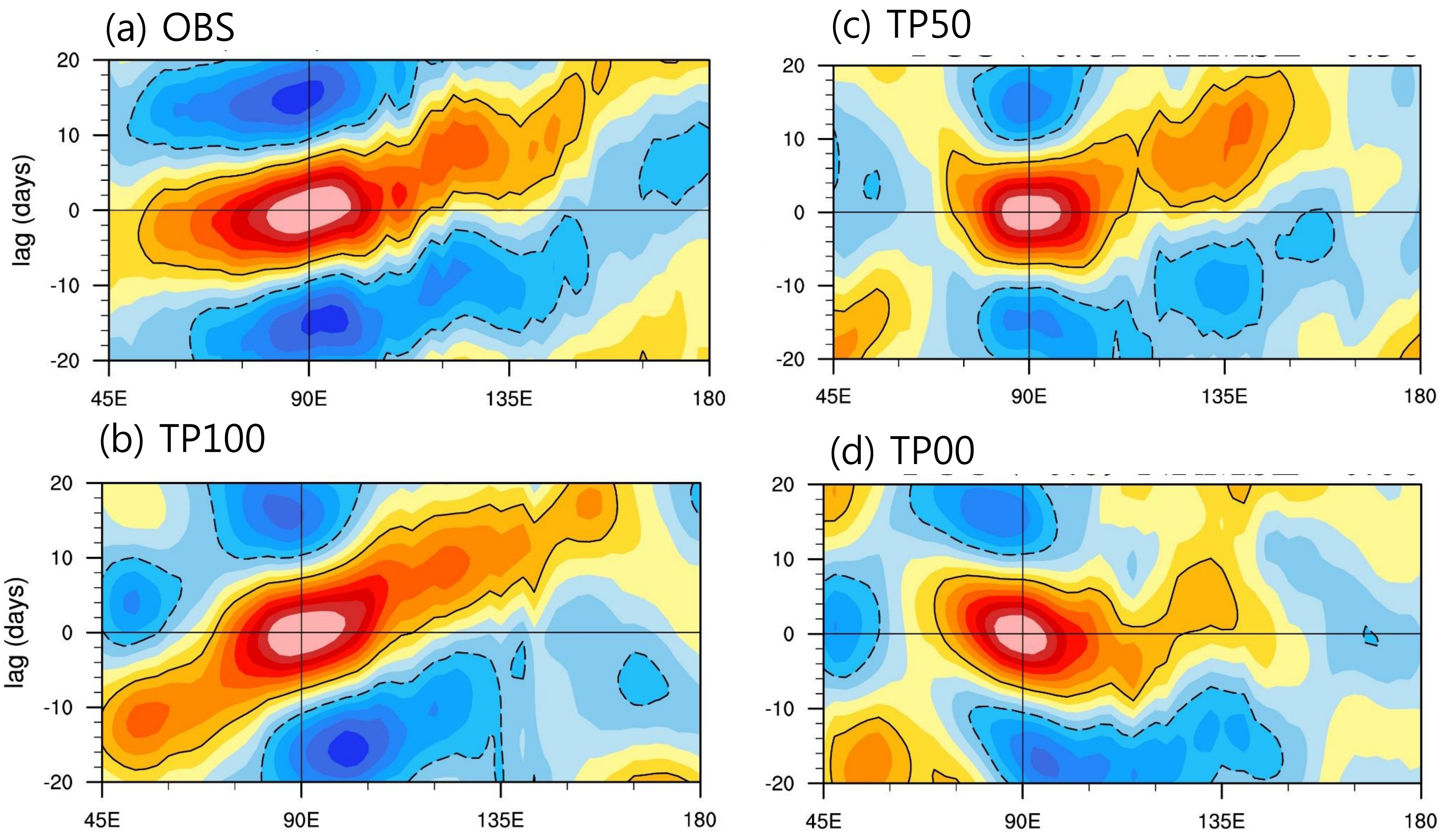

Figure S2. same as figure 2 except for the south of equatorial Indian Ocean (10°S-0°N, 80°-100°E)

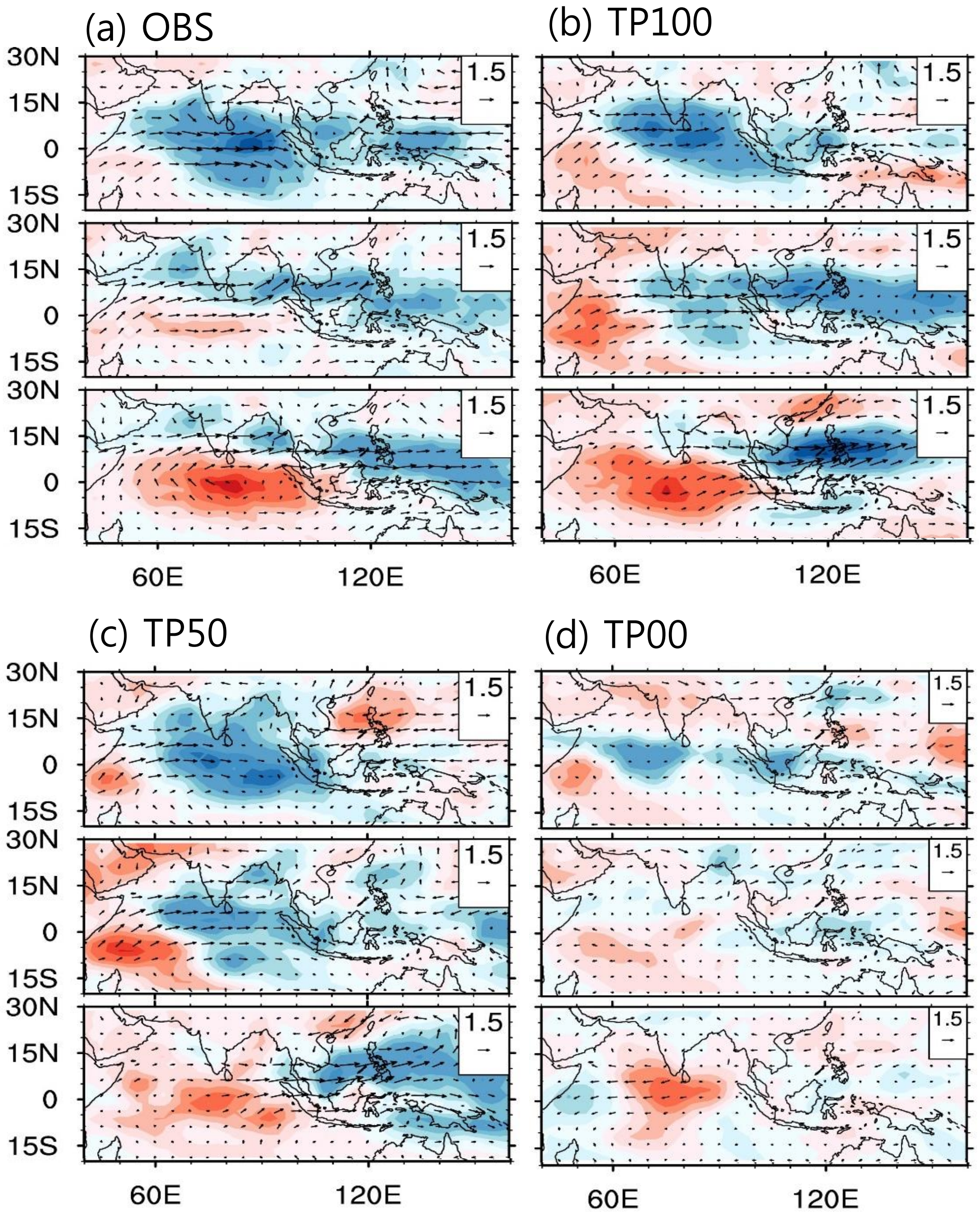

Fig. 2 The life cycle composite of OLR (shading) and 850-hPa wind (vector) anomaly reconstructed based on PC1 and PC2 of BSISO1 in 8 phases. The composite life cycles with moderate amplitude (1.0). We defined 8 phase of ISO based on Lee et al. (2013) that make its related composite fields based on the magnitudes and signs of the PC1 and PC2 of the BSISO OLR and zonal wind at 850hPa. Top (bottom) panel represents phase3 (phase 5).

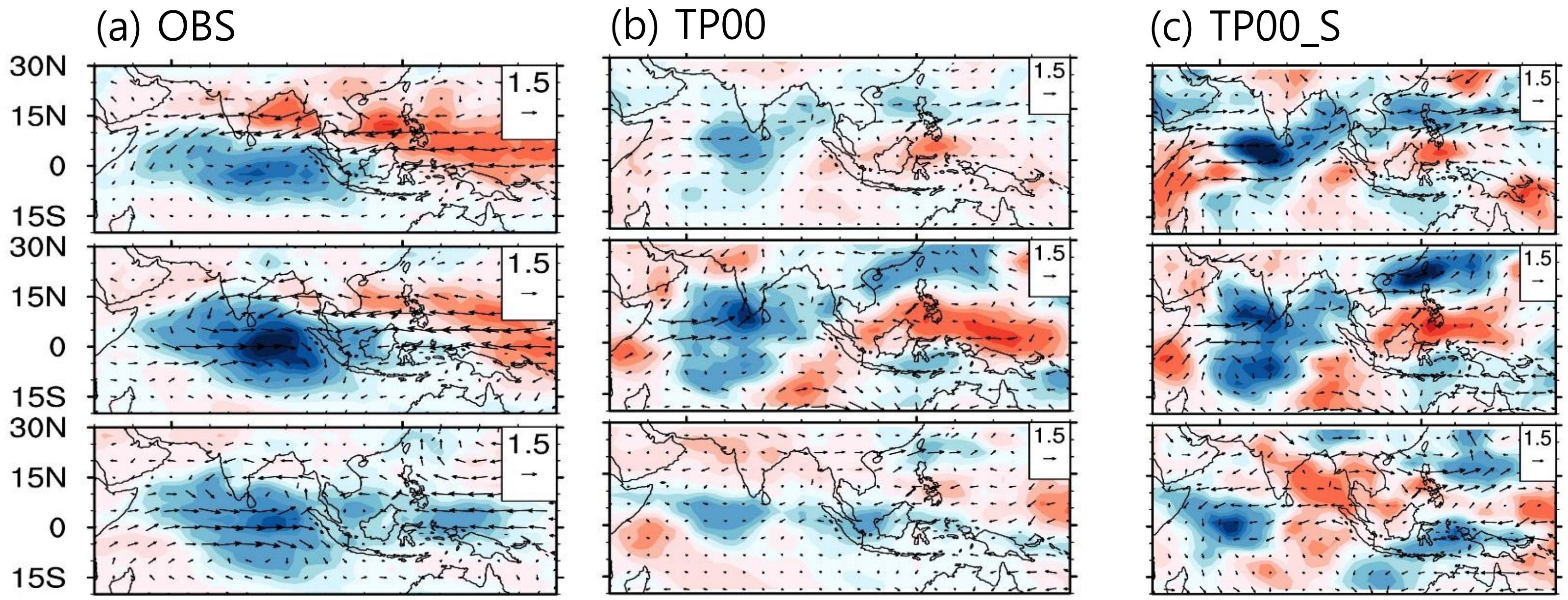

Fig. 1 The life cycle composite of OLR (shading) and 850-hPa wind (vector) anomaly reconstructed based on PC1 and PC2 of BSISO1 in 8 phases. The composite life cycles with moderate amplitude (1.0). We defined 8 phase of ISO based on Lee et al. (2013) that make its related composite fields based on the magnitudes and signs of the PC1 and PC2 of the BSISO OLR and zonal wind at 850hPa. The TP00_S represent composite of strong ISO year from all TP00 simulation data. Top (bottom) panel represents phase1 (phase 3).

Vertical profile of diabatic heating & vertical motion (arrow)

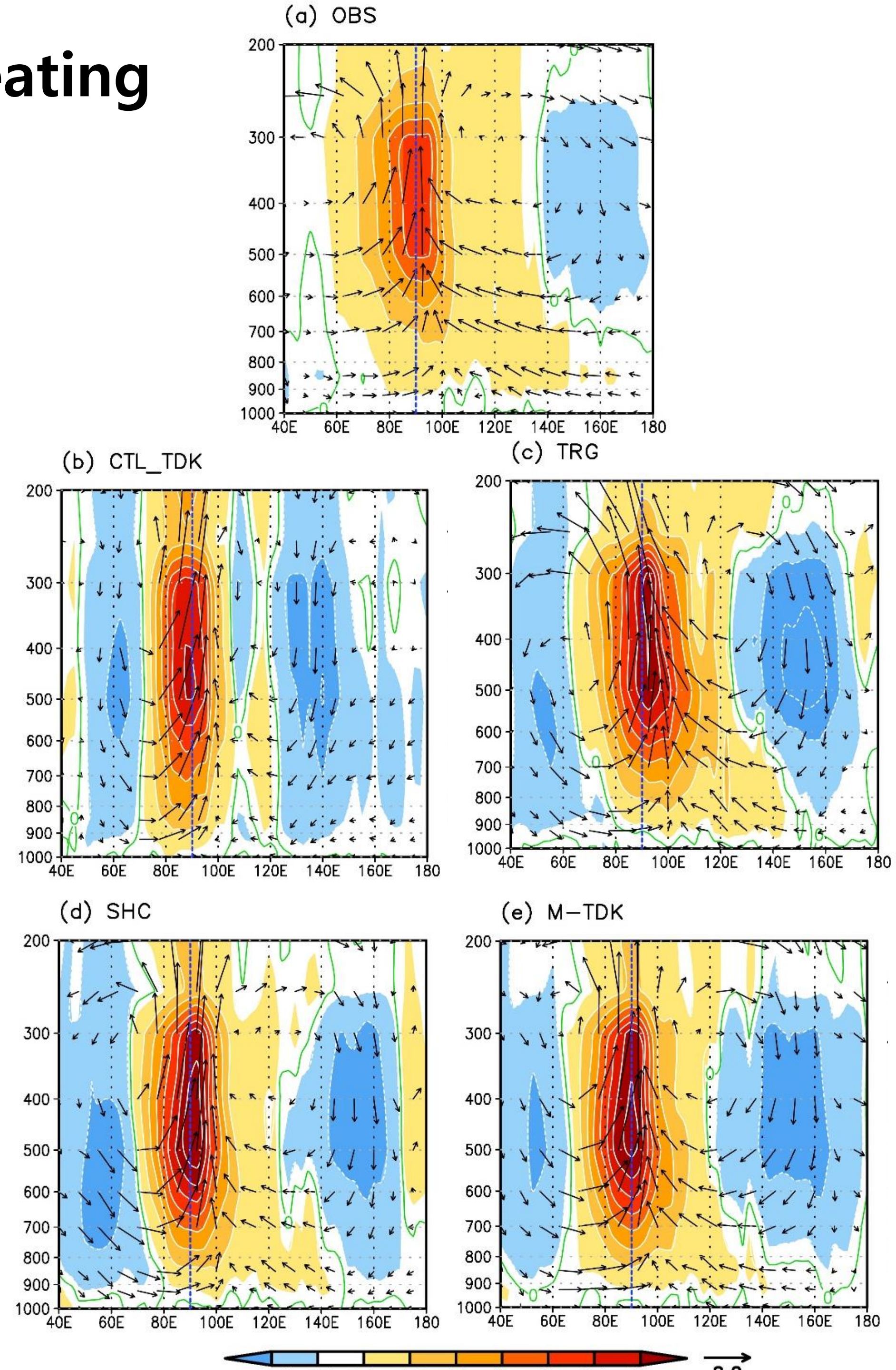

FIG.7 Equatorial zonal asymmetry in the diabatic heating (K day^{-1}, shading) and anomalous Walker cell (m s^{-1} for zonal wind and 0.01 Pa s^{-1} for the vertical velocity, vector) averaged between 5°S and 5°N in the observation (a) and model simulations (b)-(e). The structures in each panel are reconstructed using the same method as used in Fig. 6. Green contour represents the regression coefficient of 0.

Regressed convective instability (EPT : 850 hPa – 400hPa)

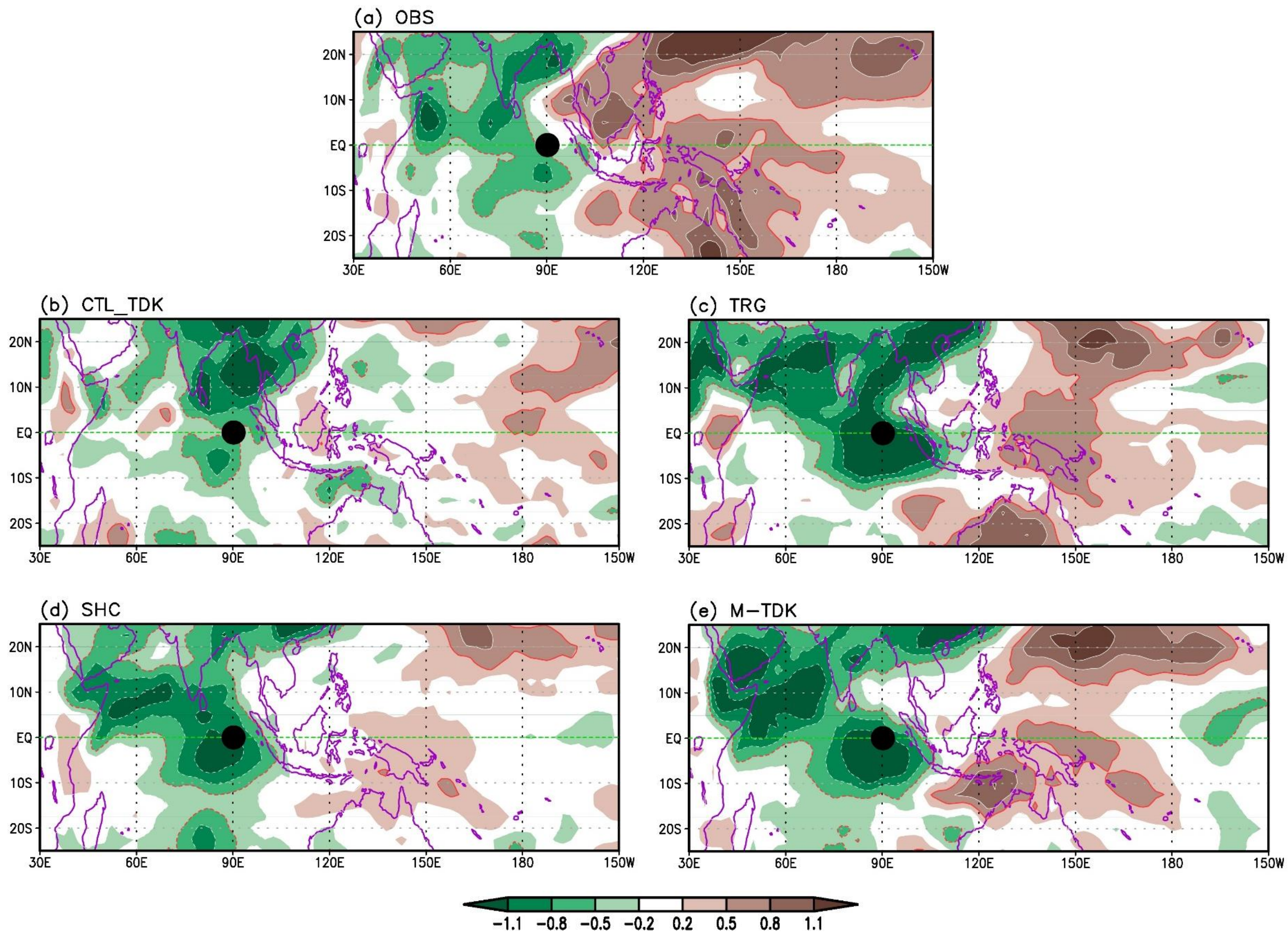

FIG.11 The same as in Fig. 3 except for the convective instability index (K). The red contour represents the regression coefficient of ±0.5.